Impact of Viscous Fingering on the Prediction of Optimum WAG Ratio

Ruben Juanes, SPE, Massachusetts Institute of Technology, and **Martin J. Blunt,** SPE, Imperial College, London

Summary

In miscible flooding, injection of solvent is often combined with water to reduce the mobility contrast between injected and displaced fluids and control the degree of fingering. Using traditional fractional-flow theory, Stalkup estimated the optimum water-solvent ratio (or WAG ratio) when viscous fingering effects are ignored, by imposing that the solvent and water fronts travel at the same speed. Here we study how the displacement efficiency and the mobility ratio across the solvent front vary with the WAG ratio when fingering is included in the analysis. We do so by computing analytical solutions to a 1D model of two-phase, three-component, first-contact miscible flow that includes the macroscopic effects of viscous fingering. The macroscopic model, originally proposed by Blunt and Christie (1993, 1994), employs an extension of the Koval fingering model to multiphase flows. The premise is that the only parameter of the model—the effective mobility ratio—must be calibrated dynamically until self-consistency is achieved between the input value and the mobility contrast across the solvent front. This model has been extensively validated by means of high-resolution simulations that capture the details of viscous fingering and carefully-designed laboratory experiments.

The results of this paper suggest that, while the prediction of the optimum WAG ratio does not change dramatically by incorporating the effects of viscous fingering, it is beneficial to inject more solvent than estimated by Stalkup's method. We show that, in this case, *both* the pore volumes injected (PVI) for complete oil recovery *and* the degree of fingering are minimized.

Introduction

Solvent flooding is a commonly used technology for enhanced oil recovery in hydrocarbon reservoirs, which aims at developing miscibility, thereby mobilizing the residual oil and enhancing the mobility of the hydrocarbon phase (Stalkup 1983; Lake 1989). Despite its high local displacement efficiency, the overall effectiveness of solvent injection may be compromised by viscous fingering, channeling, and gravity override, all of which contribute negatively to sweep efficiency (Christie and Bond 1987; Christie 1989; Christie et al. 1993; Chang et al. 1994; Tchelepi and Orr 1994). In this paper, we focus on the effect of viscous fingering; that is, the instability that occurs when a low-viscosity fluid (solvent) is injected into a formation filled with more viscous fluids (water and oil).

Mobility control of the injected solvent can be achieved by simultaneous coinjection of water—typically in alternating water and solvent slugs (WAG) (Caudle and Dyes 1958). In this way, the mobility contrast between the injected and displaced fluids is reduced, thereby limiting the degree of fingering.

There is an optimum ratio of water to solvent that maximizes recovery—in the sense of minimizing the number of pore volumes injected—while providing effective mobility control. For linear floods in homogeneous media, and without consideration of viscous fingering effects, a graphical construction of the optimum WAG ratio was given by Stalkup (1983) for both secondary floods (water/solvent injection into a medium filled with mobile oil and immobile water) and tertiary floods (water-solvent injection into a medium filled with mobile water and immobile oil). The design condition imposed in Stalkup's method is that the velocity of the water and solvent fronts be the same. Walsh and Lake (1989) performed an interesting analysis of the WAG ratio (the ratio of injected water to solvent) on the displacement efficiency for secondary and tertiary floods, using fractional-flow theory. They did not include the effects of viscous fingering, but they estimated the mobility contrast across the solvent front as a measure of the severity of fingering.

In this paper, we analyze the effect of viscous fingering on the simultaneous injection of water and solvent for secondary and tertiary oil recovery. We restrict our attention to homogeneous porous media, linear (effectively 1D) displacements, and simple phase behavior characterized by first-contact miscibility of oil and solvent. We employ the empirical viscous-fingering model proposed by Blunt and Christie (1993, 1994). They used an extension of the Koval (1963) and Todd and Longstaff (1972) models to describe fingering of the solvent in a two-phase, three-component system. They proposed a self-consistency condition to calibrate the only parameter of the fingering model—the effective mobility ratio M_{eff}. With some simplifications on the structure of the solution and the estimation of M_{eff}, analytical solutions were obtained for secondary and tertiary floods. They reported excellent agreement between analytical predictions from the empirical 1D model and averaged saturation and concentration profiles from 2D direct numerical simulations.

The results of the present paper constitute an extension of the analytical model analyzed in previous papers by the authors. Juanes and Lie (2005, 2007, in press) described the general analytical solution to the Riemann problem (constant initial and injected conditions) for the three-component, two-phase, first-contact miscible solvent system, and applied it to the simulation of 3D problems in heterogeneous reservoirs by means of streamline/front-tracking techniques. The effects of viscous fingering were ignored. Juanes and Blunt (2006) obtained analytical solutions in the presence of viscous fingering for secondary and tertiary floods, and for the entire range of water solvent injected conditions. The viscous fingering model was validated by means of high-resolution simulations that capture the details of the fingering phenomenon (Blunt and Christie 1993, 1994; Blunt et al. 1994) and by carefully designed laboratory experiments.

The main result of this paper is a series of plots that show how the number of PVI for complete oil recovery and the mobility contrast across the solvent front vary as a function of the WAG ratio. These results suggest that, while the prediction of the optimum WAG ratio does not change dramatically by incorporating the effects of viscous fingering, it is beneficial to inject more solvent than estimated by Stalkup's method. We show that, in this case, *both* the PVI for complete oil recovery *and* the degree of fingering are minimized.

Mathematical Model

We are interested in the flow through a porous medium of a mixture of three components (water, oil, and solvent) that form two distinct fluid phases (aqueous and hydrocarbon phases). We assume that water is immiscible with the two hydrocarbon components, and that oil and solvent mix readily (first-contact miscibility) to form a single hydrocarbon phase. The mathematical treatment is simplified by the assumptions that the fluids and the medium are incompressible, and that there is no volume change upon mixing of the hydrocarbon components. In addition, the

This paper (SPE 99721) was accepted for presentation at the 2006 SPE/DOE Symposium on Improved Oil Recovery, Tulsa, 22–26 April, and revised for publication. Original manuscript received for review 23 February 2006. Revised manuscript received 29 January 2007. Paper peer approved 1 February 2007.

fluid-flow dynamics are assumed to be governed by the traditional multiphase flow extension of Darcy's law, with nonhysteretic relative permeability functions. In order to render the mathematical model amenable to analysis, and to make it possible to obtain analytical solutions, we neglect the effects of gravity and capillarity. These assumptions are discussed critically elsewhere (Juanes and Blunt 2006).

Governing Equations Without Viscous Fingering. The mathematical model describing 1D flow under the previously described assumptions—and ignoring the effects of viscous fingering—is a system of two first-order conservation equations (Juanes and Lie 2005, 2007):

$$\frac{\partial S}{\partial t}+\frac{\partial f}{\partial x}=0, \quad (1)$$

$$\frac{\partial C}{\partial t}+\frac{\partial}{\partial x}\left[(1-f)\left(\frac{C}{1-S}\right)\right]=0. \quad (2)$$

In Eqs. 1 and 2, x and t are dimensionless space and time variables. Eq. 1 can be understood as the usual Buckley-Leverett equation (1942) where S is the water saturation and f is the water fractional flow. The water fractional flow is equal to the mean water velocity divided by the sum of the mean velocity of all flowing phases. Under the assumption that gravity and capillarity forces are negligible, the water fractional flow is simply the ratio of water mobility to total mobility:

$$f=\frac{\lambda_w}{\lambda_w+\lambda_h}, \quad (3)$$

where the mobility of the α-phase is defined as

$$\lambda_\alpha=\frac{k_{r\alpha}}{\mu_\alpha}, \quad (4)$$

and $k_{r\alpha}$ is the relative permeability and μ_α is the dynamic viscosity of the α-phase. Therefore, the only difference between Eq. 1 and the Buckley–Leverett equation for immiscible two-phase flow is that the hydrocarbon viscosity μ_h depends on the mass fraction of solvent χ in the hydrocarbon phase. In this paper, we have used the common quarter-power rule (Koval 1963; Todd and Longstaff 1972):

$$\mu_h=\left[\frac{1-\chi}{\mu_o^{1/4}}+\frac{\chi}{\mu_s^{1/4}}\right]^{-4}. \quad (5)$$

We shall refer to the oil/solvent viscosity ratio also as the nominal mobility ratio $M=\mu_o/\mu_s$. The relative permeability functions and the resulting water fractional-flow curves are shown in **Fig. 1** for different values of the solvent mass concentration χ in the hydrocarbon phase.

Eq. 2 expresses mass conservation of the solvent. The conservation variable C is the volume of solvent per unit pore volume. Clearly,

$$C=(1-S)\chi, \quad (6)$$

where S is the water saturation and χ is the solvent mass fraction in the hydrocarbon phase. The flux term in Eq. 2 can be understood as a "fractional flow of solvent," where $(1–f)$ is the fractional flow of the hydrocarbon phase, and $C/(1–S)=\chi$ is the mass fraction of solvent in the hydrocarbon phase.

A Viscous Fingering Model. Because of the low viscosity of the solvent, displacements associated with solvent injection may be unstable. These fluid instabilities lead, in a multidimensional scenario, to the formation and growth of fingers along the displacement front. The objective of a viscous fingering model is to capture the *averaged* behavior of the fingering phenomenon along the main flow direction, thereby allowing for a 1D description of the problem. This is illustrated in **Fig. 2.** Viscous fingering is incorporated into the formulation by an empirical model that modifies the effective solvent flux in such a way that the macroscopic effects of viscous fingering are captured. Therefore, the "solvent

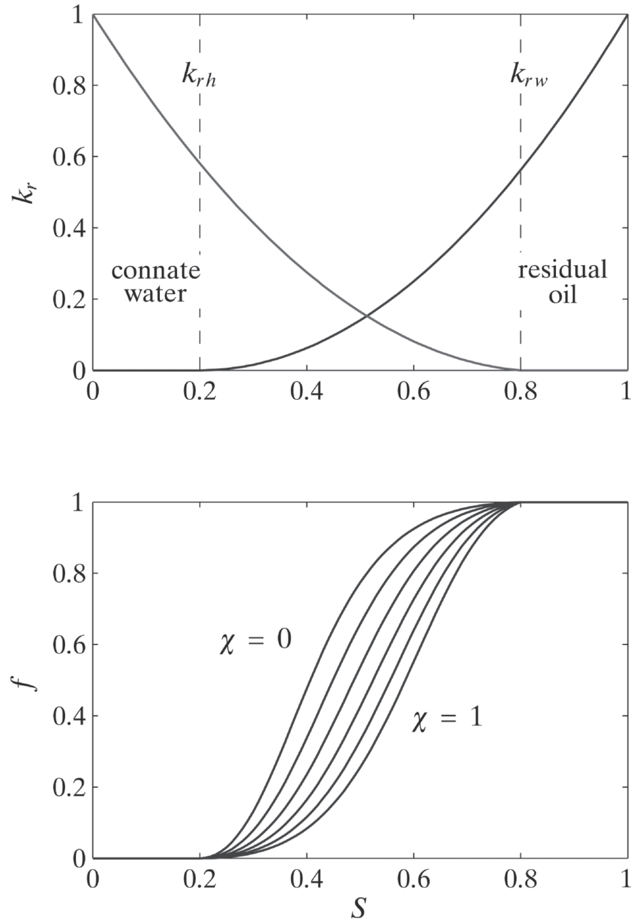

Fig. 1—Top: relative permeability functions for the water and hydrocarbon phases. Bottom: water fractional flow as a function of water saturation, for different values of the solvent mass fraction, χ=0; 0.2, . . . , 1.

flux" $(1–f)\chi$ in Eq. 2 is replaced by $(1–f)\hat{g}(\chi)$, where $\hat{g}$ is a function that attempts to capture the averaged solvent mass fraction with a 1D advective model:

$$\frac{\partial C}{\partial t}+\frac{\partial}{\partial x}[(1-f)\hat{g}(\chi)]=0. \quad (7)$$

This type of empirical model was pioneered by Koval (1963) and Todd and Longstaff (1972). They proposed the following solvent flux function (fractional flow of solvent within the hydrocarbon phase):

$$\hat{g}(\chi)=\frac{\chi}{\chi+\dfrac{1-\chi}{M_{\text{eff}}}}, \quad (8)$$

where M_{eff} is the effective mobility ratio. It is equal to one if viscous fingering is not present, and increases as viscous fingering effects become more pronounced. Different models exist to predict the value of M_{eff} given the oil and solvent viscosities. For example, Koval (1963) proposed

$$M_{\text{eff}}=(0.78+0.22M^{1/4})^4. \quad (9)$$

In this paper, we use the empirical model proposed by Blunt and Christie (1993, 1994). They used the same solvent flux function $\hat{g}(\chi)$ and effective mobility ratio M_{eff} (Eqs. 8 and 9) but dynamically calibrated the mobility ratio M. The premise is that the degree of fingering depends on the mobility contrast across the solvent front. For single-phase flows in which a first-contact miscible solvent is injected into an oil-filled medium, the mobility contrast M is equal to the viscosity ratio μ_o/μ_s. For multiphase flows, the mobility contrast is computed as the ratio of the total

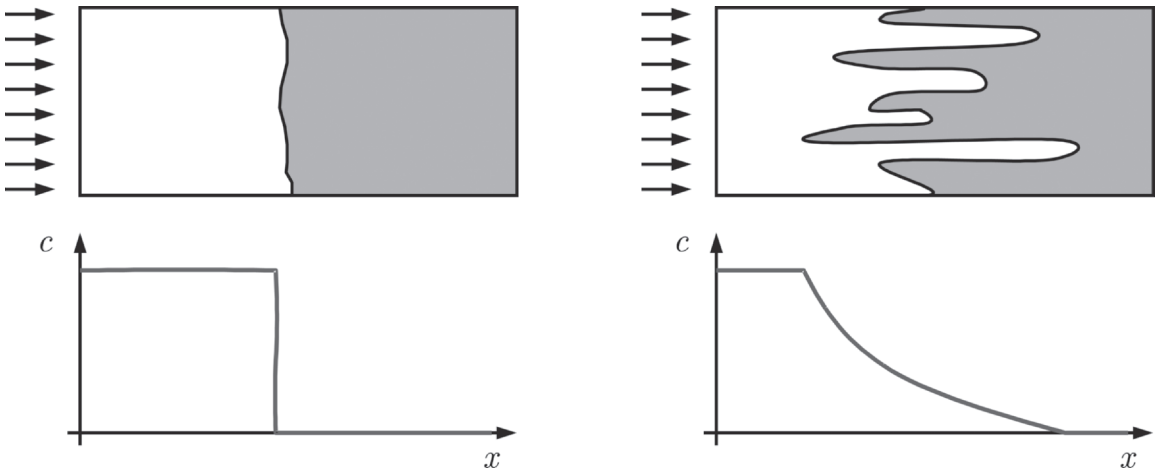

Fig. 2—Schematic of a stable displacement (left) and an unstable displacement that develops viscous fingering (right).

mobility immediately upstream and immediately downstream of the solvent front:

$$M = \frac{\lambda_T^{\text{up}}}{\lambda_T^{\text{down}}}. \quad \ldots\ldots\ldots\ldots\ldots\ldots\ldots\ldots\ldots\ldots\ldots\ldots\ldots\ldots\ldots\ldots (10)$$

The effective mobility ratio M_{eff} can then be calculated by inserting this value of M into Eq. 9. Obviously, the value of the effective mobility ratio affects the solution, and an iterative scheme is required to achieve consistency between the *input* effective mobility ratio $M_{\text{eff}}^{\text{in}}$ and the *output* $M_{\text{eff}}^{\text{out}}$ obtained from Eqs. 10 and 9 once the solution is computed.

Composition Diagrams. The model given by Eqs. 1 and 2 (or Eqs. 1 and 7 if viscous fingering is modeled) must be supplemented with initial and boundary conditions. We are interested in the solution to the Riemann problem; that is, the solution in an unbounded domain where the initial conditions are simply two constant states (left or injected state $[S_l, C_l]$, and right or initial state $[S_r, C_r]$) separated by a single discontinuity at $x = 0$. The Riemann problem approximates common experimental and field conditions, in which the initial saturations and compositions are uniform and the injected conditions are held constant in time.

At any point in space and time, the solution vector $[S,C]$ must lie on the unit triangle:

$$U \equiv \{[S, C]: S \geq 0, C \geq 0, S + C \leq 1\}, \quad \ldots\ldots\ldots\ldots\ldots\ldots\ldots\ldots\ldots\ldots (11)$$

that is, the water saturation (S), the overall solvent volume fraction (C), and the overall oil volume fraction ($1–S–C$) must be between 0 and 1. This unit triangle representing water saturation and solvent concentration is called the phase (or composition) space.

The system of equations and the initial condition are invariant under uniform stretching of coordinates $(x, t) \mapsto (cx, ct)$ with $c>0$, which means that the solution $[S(x,t), C(x,t)]$ does not depend on x and t independently but, rather, on the similarity variable $\zeta = x/t$ (the characteristic speed). If the solution is known at a given time, it is automatically known at any other time by simple rescaling. Therefore, the solution can be interpreted as a route on the phase space, from the injected state to the initial state (Helfferich 1981; Pope 1980). The entire route is composed of a sequence of waves connecting injected and initial states and, possibly, other intermediate constant states. Each wave has a corresponding characteristic velocity, which must increase from the injected to the initial state. There are various types of wave, including continuous (rarefaction) waves, discontinuous self-sharpening (shock) waves, and discontinuous indifferent (contact) waves (Smoller 1994). Juanes and Lie (2007) provide a complete analysis of the system without viscous fingering by drawing an analogy with the polymer system (Isaacson 1980), and Juanes and Blunt (2006) do the same for the system that includes viscous fingering. That analysis, which includes a study of the mathematical character of the system of equations, a description of the different waves that may arise, and a complete classification of the Riemann solution, will not be repeated here. We illustrate, however, some of the important differences between the two models in terms of the so-called composition diagram. The composition diagram is a representation of potentially admissible continuous (rarefaction) waves on the phase space. Although this information alone is insufficient to construct solutions to the Riemann problem (because shock curves and rarefaction curves do not coincide, in general), it does provide a good idea of what type of saturation/composition variations one may expect. In the case of a hyperbolic system of two equations, these curves are organized into two families, each associated with the slow or fast characteristic family (Smoller 1994).

In **Fig. 3,** we show the composition diagram for the system without viscous fingering. The slender continuous lines correspond to waves in which water saturation changes and the solvent mass fraction χ remains constant: waves of the S-family, also called tie-lines in fractional flow theory (Helfferich 1981). The discontinuous curves are associated with waves in which the solvent mass fraction changes: waves of the C-family or nontie-lines. It turns out that these are indifferent waves (contact discontinuities); the characteristic speed is constant along them. The thick black curve denotes the transition curve: a line along which the charac-

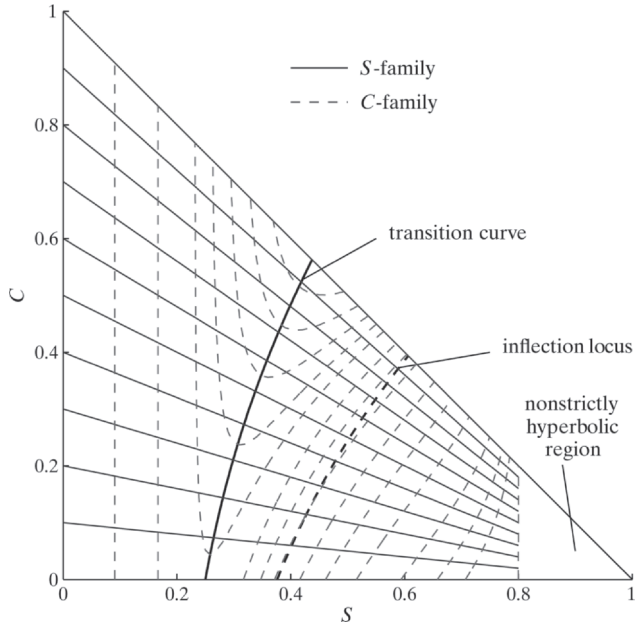

Fig. 3—Composition diagram for the system with no viscous fingering.

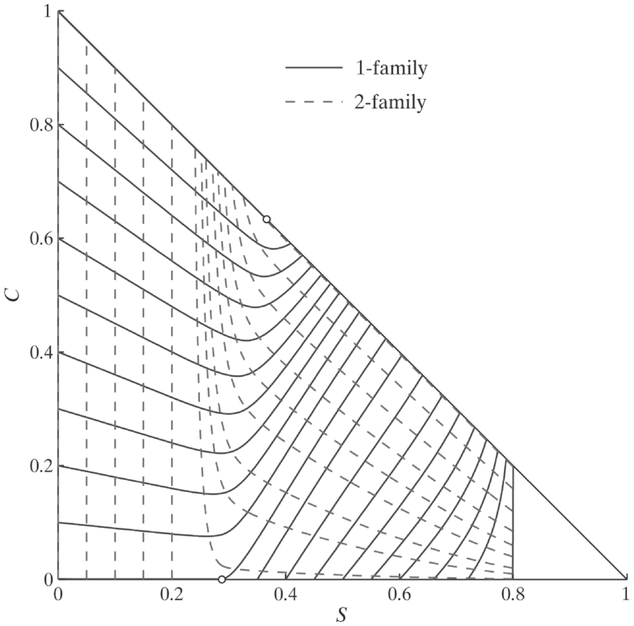

Fig. 4—Composition diagram with viscous fingering, for the nominal mobility ratio M=10 (M_{eff}≈1.88).

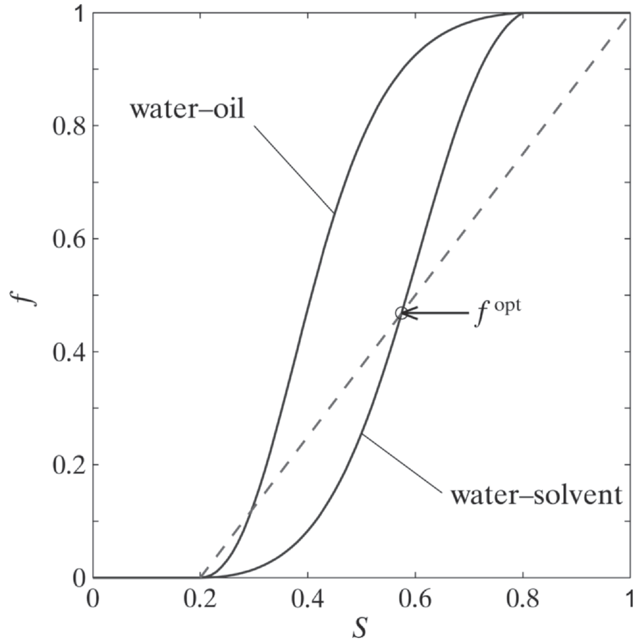

Fig. 5—Stalkup's method for the prediction of optimum WAG ratio in secondary floods.

teristic speeds of S-waves and C-waves are the same. To the left of the transition curve, the wave speed of tie-lines is lower than that of the nontie-lines, while the wave speed of tie-lines is higher than that of nontie-lines to the right of the transition curve. Therefore, the two characteristic families change order as the transition curve is crossed.

For the system that accounts for viscous fingering, the precise form of the composition diagram depends on the effective mobility ratio M_{eff} which, in turn, depends on the mobility ratio M through Koval's formula. The composition diagram (integral curves of slow and fast eigenvectors) is shown in **Fig. 4** for an oil/solvent viscosity ratio $M=10$, for which the effective mobility ratio is $M_{eff} \approx 1.88$. The composition diagram is similar to that of the case with no viscous fingering, but with some notable differences: (1) there is no transition curve but, rather, a whole region in which tie-line paths effectively switch to nontie-line paths; (2) waves associated primarily with changes in water saturation are no longer straight lines; and (3) waves associated primarily with changes in composition no longer correspond to curves of constant characteristic speed.

Prediction of Optimum WAG Ratio

The WAG ratio is defined as the ratio of injected water to injected solvent, both expressed in reservoir volumes:

$$W_R = \frac{f_{inj}}{1 - f_{inj}}, \quad (12)$$

where f_{inj} is the water fractional flow of the injected conditions. In this section, we revisit the classical method for estimating the optimum WAG ratio in the absence of viscous fingering due to Stalkup (1983). We provide an interpretation of Stalkup's method from the point of view of the composition diagram, and extend the analysis for the prediction of the optimum WAG ratio when the governing equations include viscous fingering.

Stalkup's Method. There is an optimum WAG ratio at which the number of pore volumes injected required for 100% recovery of the oil is minimized while, at the same time, reducing the mobility contrast across the solvent front and therefore limiting the degree of fingering.

A graphical construction for the evaluation of the optimum WAG ratio in secondary and tertiary floods was first given by Stalkup (1983) when viscous fingering is not included in the analysis. The premise is that, for these injected conditions, the water and solvent fronts travel at the same speed. A careful and elegant analysis using fractional flow theory is given by Walsh and Lake (1989).

Stalkup's graphical construction is reproduced in **Fig. 5** for the case of secondary floods; that is, when the reservoir is initially filled with mobile oil and connate (immobile) water. The injected conditions can be represented as a point on the water/solvent fractional flow curve. The slope of the straight line from point (1,1) to the injected conditions (S_{inj}, f_{inj}) corresponds to the speed of the solvent front. The slope of the straight line from the injected state to the initial state (S_{wc}, 0) is the speed of the water shock. The optimum injected conditions are those for which both slopes are the same, as shown in Fig. 5.

The graphical construction for obtaining the optimum WAG ratio in tertiary floods is slightly more complicated (see **Fig. 6**). In

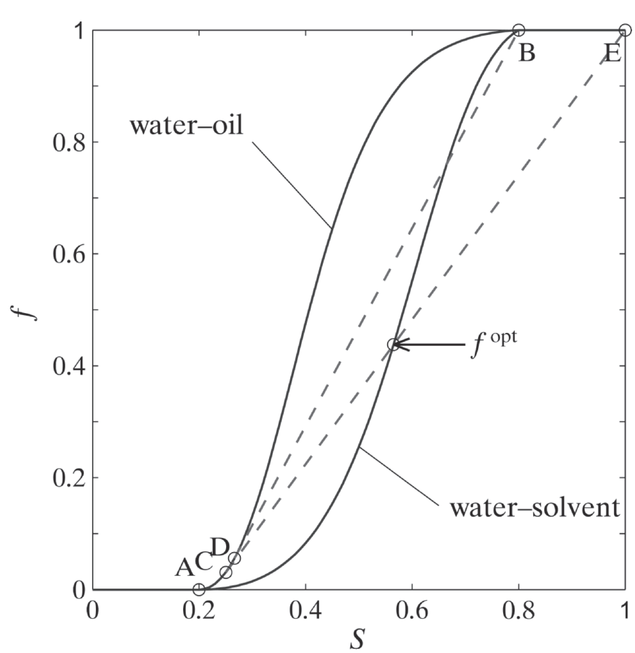

Fig. 6—Stalkup's method for the prediction of optimum WAG ratio in tertiary floods.

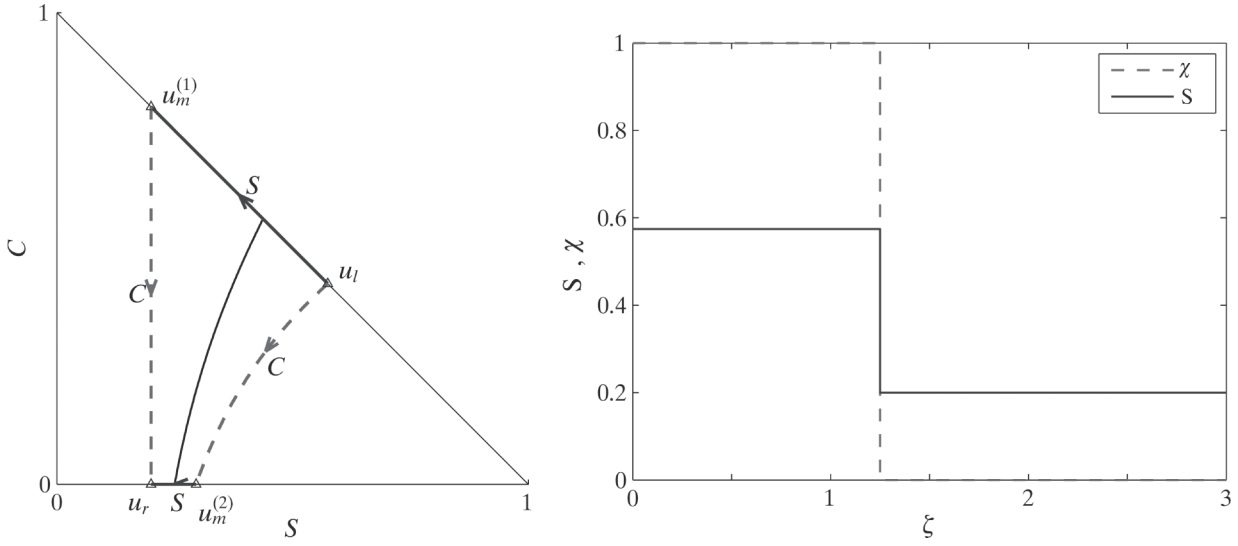

Fig. 7—Interpretation of Stalkup's method for secondary floods, and corresponding solution profile.

this case, the initial state of the reservoir corresponds to residual oil after waterflood (point B). As before, the injected conditions can be represented as a point on the water/solvent fractional flow curve. It turns out that, in this case, the fast wave is always a Buckley-Leverett shock, the speed of which is computed by drawing the tangent from point B to the water/oil fractional-flow curve (point D). If the WAG ratio is below optimal, there will be two waves behind this fast Buckley-Leverett shock: a water front and a solvent front. The speed of the solvent front corresponds to the slope of the straight line from point (1,1) to the tangent of the water/oil curve (point C). The speed of the water front is given by the slope of a straight line from the injected conditions (S_{inj}, f_{inj}) to the intersection of the water/solvent curve with the extension of the straight line EC. Both fronts (the water front and the solvent front) will have the same speed when the injected conditions are precisely at the intersection of the straight line EC with the water/solvent fractional flow curve. This optimum is shown in Fig. 6 and is, in general, different from the secondary flood optimum.

Interpretation of Stalkup's Method. Stalkup's method for predicting the optimum injected conditions can be reinterpreted as the point for which a bifurcation in the solution occurs on the phase diagram.

Consider secondary floods first. The initial state is $u_r = [S_r, C_r] = [S_{wc}, 0]$ and the injected state will be a state $u_l = [S_l, C_l]$ somewhere along the diagonal of the unit triangle (because no oil is injected). The solution on the phase diagram will be a combination of waves connecting the injected state to the initial state. If the amount of injected water is low, the solution will be of the type *SC*: a sequence of a slow water shock from the injected state u_l to an intermediate state $u_m^{(1)}$, and a fast solvent front from $u_m^{(1)}$ to the initial state u_r. In contrast, if the amount of injected water is high, the solution will consist of a slow solvent front from the injected state u_l to an intermediate state $u_m^{(2)}$, and a faster water shock displacing the oil that connects the intermediate state $u_m^{(2)}$ with the initial state u_r (solution of type *CS*). The two types of solution have markedly different paths on the phase diagram. There is, in fact, an injected state for which the solution bifurcates, representing the transition between the two types of solution (see **Fig. 7**). This state is precisely the one for which the *S*-wave and the *C*-wave travel at the same speed and, therefore, corresponds to Stalkup's definition of optimum injected state. The profiles of water saturation *S* and solvent mass fraction χ in the hydrocarbon phase are shown on the right plot of Fig. 7, where it is evident that the speeds of both waves are the same. It should be noted that, despite the fact that bifurcation occurs on the phase diagram, the solution shows continuous dependence on the injected conditions in physical space. That is, the saturation and concentration profiles vary continuously with changes in the injected conditions.

Similar arguments apply to tertiary floods. The initial state is now $u_r = [S_r, C_r] = [1 - S_{or}, 0]$ and the injected state $u_l = [S_l, C_l]$ is on the diagonal edge of the unit triangle. If the injected water saturation is low, the solution consists of a sequence of three waves: a slow water shock *S* from u_l to an intermediate constant state $u_m^{(1)}$, preceded by a faster solvent front *C* that connects $u_m^{(1)}$ to a tangent shock state u_t, which is itself preceded by a faster Buckley-Leverett water shock *S* from u_t to the initial state u_r. On the other hand, if the amount of water injected is sufficiently high, the slower water and solvent fronts merge onto one single traveling discontinuity, which we still denote as a solvent front *C*. Bifurcation between these two solution types occurs for an injected state such that the slow *S*- and *C*-waves have the same speed, as shown in **Fig. 8.** Also shown in Fig. 8 are the water saturation and solvent concentration profiles which, once again, emphasize the fact that the water and solvent fronts travel with the same speed.

Including Viscous Fingering. Analytical solutions to the Riemann problem are much more complex when viscous fingering effects are incorporated into the model. They have been fully characterized, however, for secondary and tertiary floods (Juanes and Blunt 2006). The additional complexity in the treatment of the multiphase first-contact miscible model with viscous fingering comes from the following:

1. The wave paths associated with changes in solvent concentration are no longer contact discontinuities; that is, they do not have a constant wave speed.

2. For tertiary floods, the shock curves present detached (nonlocal) branches. This leads to scenarios in which the slower solvent front and the faster Buckley-Leverett shock interact, or, in other words, the solvent front pushes through, destroying the oil bank. The result of that interaction is a leading shock that involves changes in *both* water saturation and solvent mass fraction. Interestingly, this feature explains why in miscible tertiary floods, oil and solvent often break through simultaneously.

3. Evaluation of the solution requires that the correct value of the effective mobility ratio be used. Iteration is needed to achieve self-consistency between the input and output values of the mobility contrast across the solvent front. Quite often, the structure of the solution is very sensitive to the value of the effective mobility ratio, and implementation of a robust iterative algorithm is therefore a challenge. We discuss this issue further in the Discussion and Conclusions section.

Stalkup's construction results in injected states that satisfy the following property: they maximize the water-to-solvent ratio of the mixture, while simultaneously minimizing the number of pore volumes injected required for 100% oil recovery. In the previous subsection, we saw that the model without viscous fingering leads

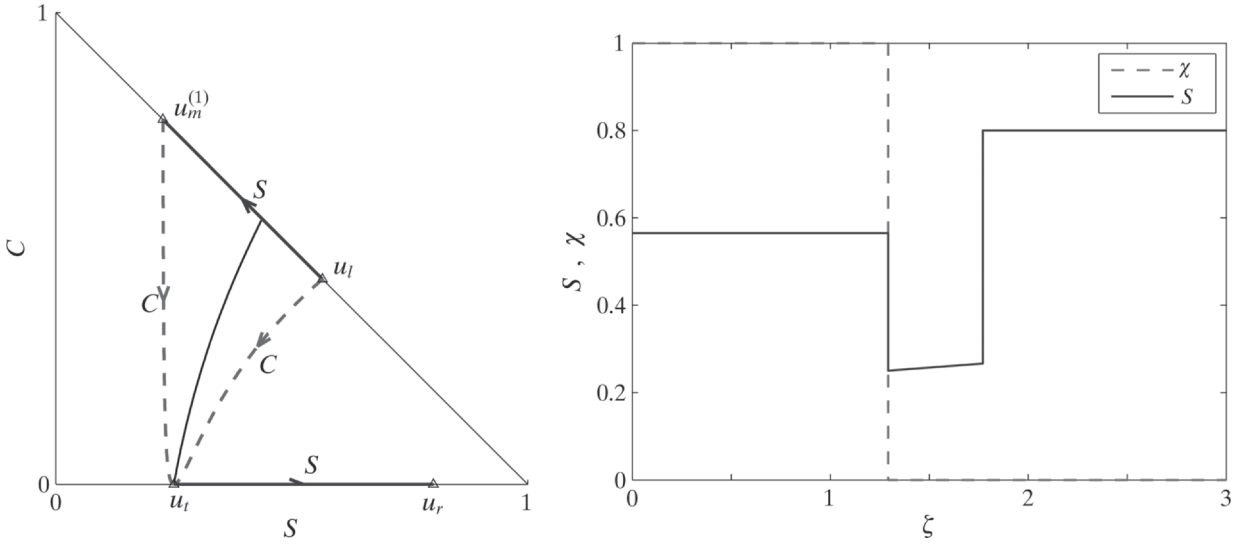

Fig. 8—Interpretation of Stalkup's method for tertiary floods, and corresponding solution profile.

to bifurcation of the solution in phase space. This is not the case when viscous fingering effects are incorporated: the solution depends continuously on the initial data both on physical and phase space (Juanes and Blunt 2006). Therefore, bifurcation of the solution cannot be used as a criterion for the definition of the optimum WAG ratio. However, we can still define the optimum WAG ratio as the injected state that minimizes the number of pore volumes injected for complete recovery of the oil in place.

To illustrate the differences in the solution when viscous fingering effects are included, we show in **Figs. 9 and 10** the composition path, the saturation and composition profiles, and the total mobility profile for the optimum injected state in secondary and tertiary floods, respectively. The solutions with viscous fingering follow composition paths that are somewhere in between the two bifurcation solutions of the model without viscous fingering. There are notable dissimilarities between them, however. For example, the solvent fronts in the solutions with viscous fingering are rarefaction waves that reflect the dispersive nature of viscous fingering. The added benefit of including viscous fingering in a self-consistent fashion is that predictions are performed using the mobility contrast across the front and, therefore, accounting for the degree of fingering that actually takes place.

Impact of Viscous Fingering

In this section, we compile the main results of the paper, in the form of plots of the number of pore volumes injected (PVI) required for 100% recovery and mobility contrast across the solvent front, as a function of the injected water fractional flow. Each

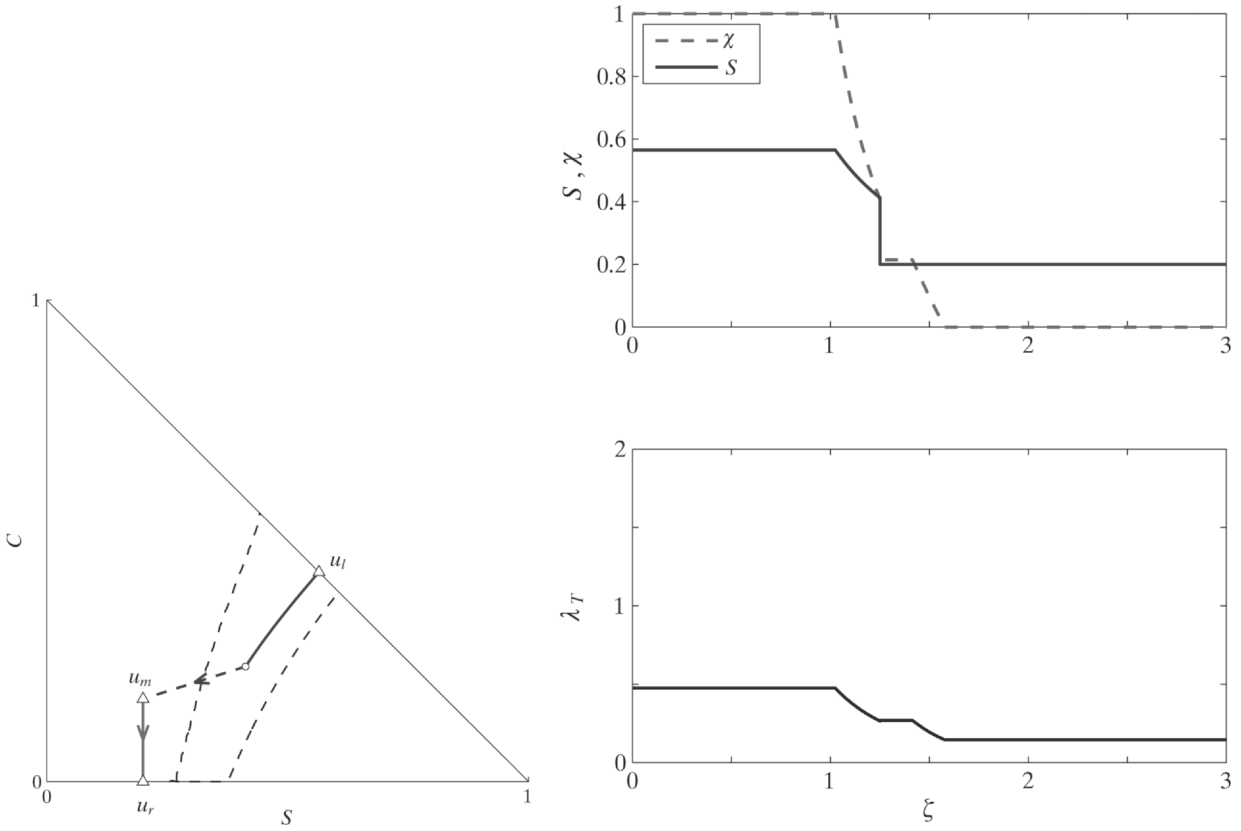

Fig. 9—Composition path and composition profiles at the optimum injected WAG ratio for secondary floods.

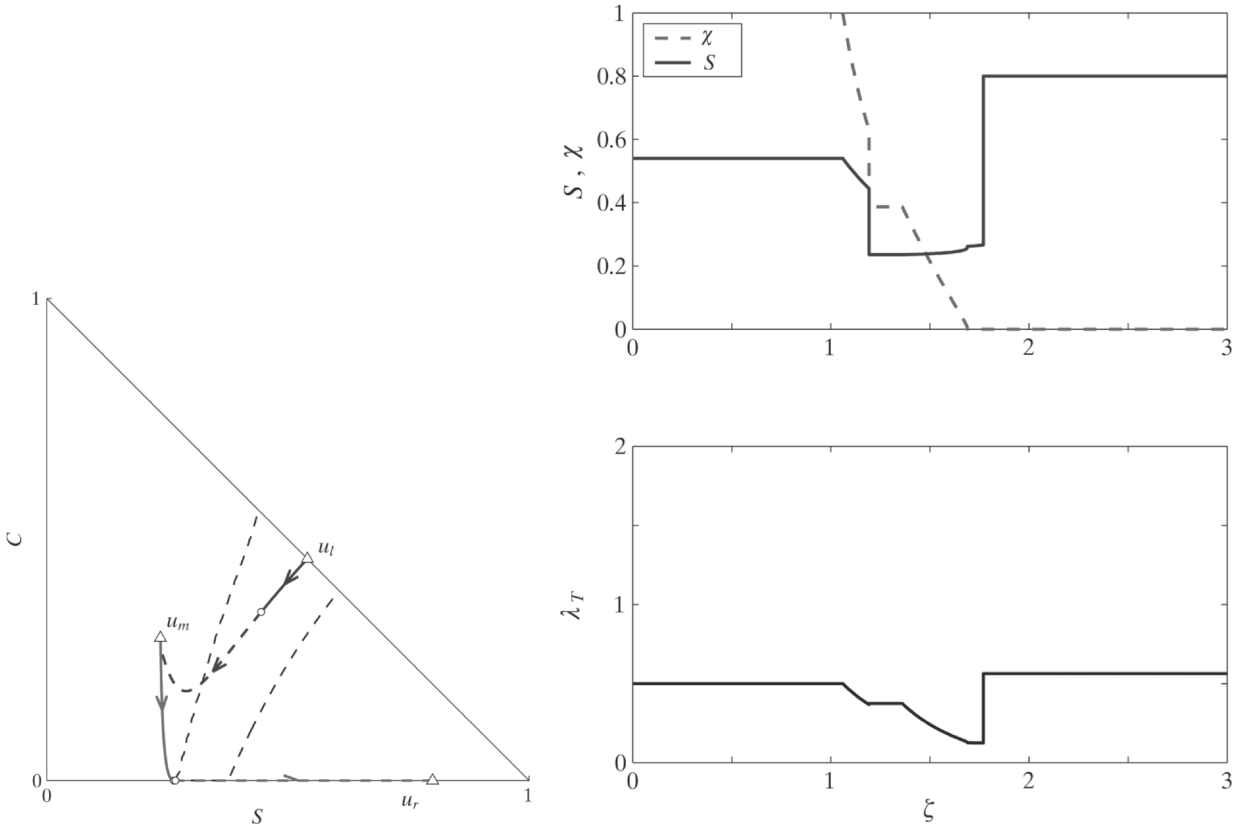

Fig. 10—Composition path and composition profiles at the optimum injected WAG ratio for tertiary floods.

individual solution of these curves was obtained by iterating on the mobility ratio to achieve self-consistency, as explained earlier. We also compare the new predictions with those obtained when viscous fingering is neglected, therefore complementing the analysis of Walsh and Lake (1989), where viscous fingering was not included.

Moderate Viscosity Ratio. In **Fig. 11,** we plot the PVI for 100% recovery (bottom) and the corresponding mobility contrast across the solvent front (top) as a function of the injected water fractional flow, for simultaneous water/solvent *secondary floods*. We compare the results of the models with and without viscous fingering when the nominal mobility ratio (oil/solvent viscosity ratio) is equal to 10.

The model without viscous fingering predicts that the displacement efficiency and the mobility ratio across the solvent front remain unchanged for $0<f_{\mathrm{inj}}<f_{\mathrm{inj}}^{\mathrm{crit}}$. At this critical $f_{\mathrm{inj}}^{\mathrm{crit}}$ the mobility ratio drops from a value of exactly 10 to a much lower value of approximately 4. For $f_{\mathrm{inj}}<f_{\mathrm{inj}}^{\mathrm{crit}}$ the mobility ratio continues to decrease, but the displacement efficiency also decreases as W_R increases (more PVI are required to recover all the oil). In this classical analysis, the optimum WAG ratio (which coincides with the value obtained by Stalkup's method) is then taken as a value slightly greater than the critical value, $W_R\approx 0.88$ in this case, because it combines the highest displacement efficiency PVI = 0.80 with a relatively low value of the mobility contrast.

The model with viscous fingering, on the other hand, predicts a continuous dependence of the displacement efficiency and the *self-consistent* mobility ratio across the solvent front with respect to the water/solvent ratio. The curves of PVI and mobility ratio both show a minimum at approximately the same water fractional flow. The minimum of the PVI curve corresponds to $W_R\approx 0.78$, for which PVI≈0.93.

In **Fig. 12,** we perform the same analysis for *tertiary floods*, with similar observations. The model without viscous fingering predicts a constant mobility contrast and PVI for 100% recovery for WAG ratios below the Stalkup optimal, and a progressive increase in PVI together with a decrease in mobility contrast for WAG ratios above the Stalkup optimal. From this analysis that ignores viscous fingering, one would choose a WAG ratio slightly above the critical value $W_R\approx 0.78$, for which PVI≈0.77. The model predictions that account for viscous fingering predict, on the other hand, a lower value of the optimal WAG ratio, $W_R\approx 0.56$, and a higher value of the associated PVI≈0.94.

Severe Viscosity Ratio. A relevant question is whether the discrepancy in the predictions between the models with and without viscous fingering is heavily dependent on the nominal mobility ratio. Intuitively, it seems reasonable to think it is and that, for severe oil/solvent viscosity ratios, the two models will yield very different predictions. We address this question by repeating the previously described analysis with a higher viscosity ratio, $M = 100$.

The results for tertiary floods are shown in **Fig. 13.** Note that the plot of the mobility contrast across the solvent front has a semilog scale. When comparing the two models, it is apparent that, for low WAG ratios, the model that ignores viscous fingering severely overestimates the mobility contrast across the front and significantly underestimates the PVI for 100% recovery. This is to be expected, because this is the range of injected conditions (too much solvent) for which viscous fingering plays a dominant role.

However, when the WAG ratio is sufficiently high, the differences between the two models are reduced. The fractional flow model that ignores viscous fingering yields an optimum WAG ratio of $W_R\approx 2.13$ (equal to the Stalkup optimum) and an associated PVI≈0.77. The model that accounts for viscous fingering in a self-consistent fashion predicts a lower optimum WAG ratio, $W_R\approx 1.45$, with PVI≈0.90 for 100% recovery. While the discrepancy between models is larger than for $M = 10$, it is less pronounced than what one might have anticipated given the large value of the oil/solvent viscosity ratio.

Discussion and Conclusions

The results of the previous section display several general trends.

1. The first observation is that the estimates of the optimum WAG ratio that account for viscous fingering are lower than those that

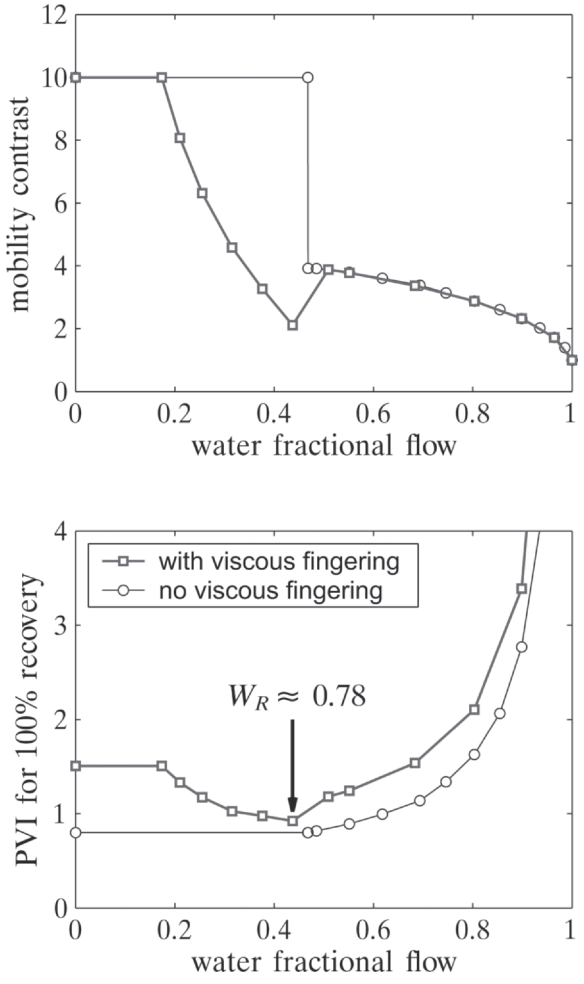

Fig. 11—Mobility contrast and pore volumes injected for 100% recovery as a function of the injected water fractional flow. Secondary floods.

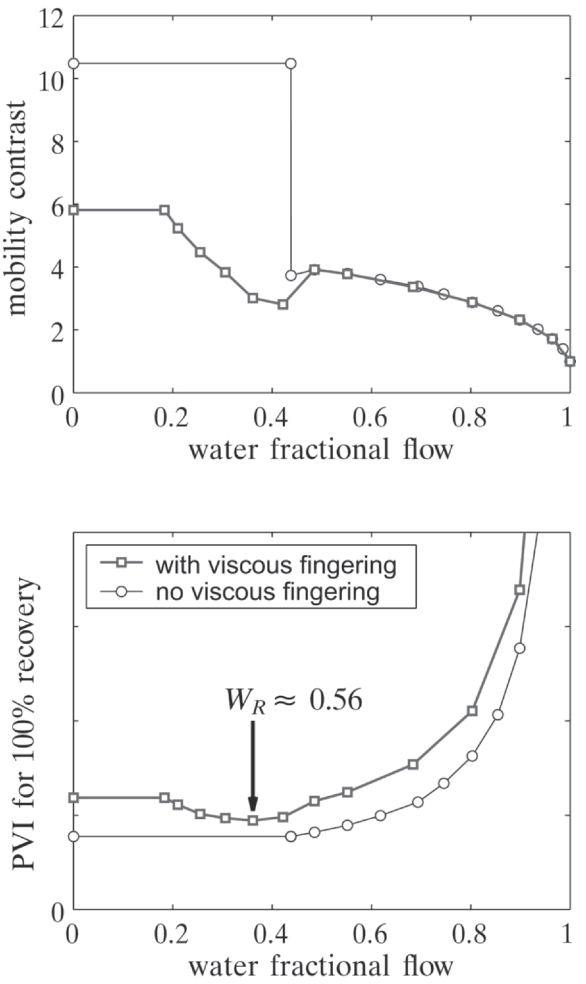

Fig. 12—Mobility contrast and pore volumes injected for 100% recovery as a function of the injected water fractional flow. Tertiary floods.

ignore viscous fingering effects. This means that the number of PVI for complete oil recovery is minimized by injecting a higher solvent fraction than predicted by the Stalkup method. What is more, the self-consistent minimum in the mobility contrast displays a minimum for WAG ratios below the Stalkup optimum, indicating that it is safe to inject more solvent, and that the measure of the degree of fingering predicted by the classical fractional-flow theory (Walsh and Lake 1989) is unreliable.

2. The solutions without viscous fingering display bifurcation in phase space and discontinuous behavior in the mobility contrast across the solvent front as the injected water fractional flow changes. This is not the case for the solutions with viscous fingering: the composition route varies continuously as a function of the injected state, and so does the self consistent mobility ratio. To reiterate this point, we plot in **Fig. 14** the variation of the Todd and Longstaff (1972) parameter ω as a function of the injected water fractional flow for both secondary and tertiary floods. This parameter can be computed directly by using the definition of the effective mobility ratio proposed by Todd and Longstaff (1972):

$$M_{\text{eff}} = M^{1-\omega}, \quad \ldots\ldots\ldots\ldots\ldots\ldots\ldots\ldots\ldots\ldots\ldots\ldots\ldots\ldots (13)$$

together with Eq. 9, to yield

$$\omega = 1 - \frac{\log M_{\text{eff}}}{\log M} = 1 - 4\,\frac{\log(0.78 + 0.22M^{1/4})}{\log M}. \quad \ldots\ldots (14)$$

The Todd and Longstaff parameter ω serves also as a measure of the degree of fingering. It is equal to 1 if fingering is completely suppressed, and a lower value indicates more fingering. From this figure, it is apparent that ω is continuously varying with the injected conditions. There are significant discrepancies between this figure and the corresponding figure (Fig. 11) in the study of Blunt and Christie (1993). Without going into all the details, the differences can be attributed to the following factors, all of them ignored or simplified by Blunt and Christie (1993):

(a) The intermediate constant state of the solution may be well inside the composition triangle, and not on the water-solvent edge or the water-oil edge (see Figs. 9 and 10).

(b) The solution involves in fact two solvent fronts and, therefore, two values of the mobility contrast given by Eq. 10. The presence of two solvent fronts with different mobility contrast is evident from the mobility profiles in Figs. 9 and 10. If the injected mixture is rich in solvent, M associated with the fast solvent front (red curve in Figs. 9 and 10) is larger. As a higher fraction of water is injected, there is a crossover, and M associated with the slow front (blue curve) is larger. It is the larger value of M that is used to iterate on the self-consistent M_{eff}, something that was not accounted for by Blunt and Christie (1993). This also explains why M_{eff} (and thus the Todd and Longstaff parameter ω) should be the same for secondary and tertiary floods if the fraction of water injected is large enough: in this case, M from the slow front dominates and the slow wave is actually identical for both secondary and tertiary floods (Juanes and Blunt 2006).

As a result, Blunt and Christie (1993) predict a monotonic curve of ω vs. injected water fractional flow, a discontinuity in ω at the optimum WAG ratio, and very high values of ω above the optimum. In contrast, we predict nonmonotonic (but continuously varying) ω with f_{inj}, and relatively low values of ω (lower than 0.8) throughout.

3. Because the solvent fingers through, the displacement is less efficient than predicted by the model that neglects viscous fin-

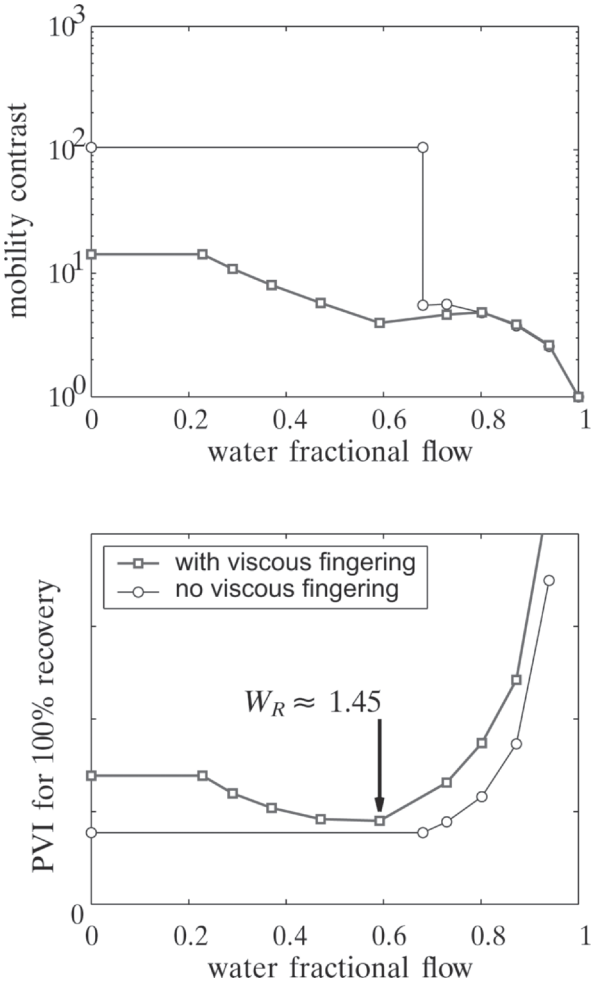

Fig. 13—Mobility contrast and pore volumes injected for 100% recovery as a function of the injected water fractional flow. Tertiary floods with severe viscosity ratio *M*=100.

gering. Thus, the PVI required for complete recovery of the oil is always larger in the model that accounts for viscous fingering.

4. The models with and without viscous fingering differ only marginally with regard to the predictions of optimum WAG ratio, even for cases with severe viscosity ratio. The reason is that near the optimum WAG ratio, the mobility contrast across the solvent front is much lower than the nominal mobility ratio. However, as noted earlier, the results of this paper suggest that it is beneficial to inject a higher fraction of solvent than predicted by Stalkup's method.

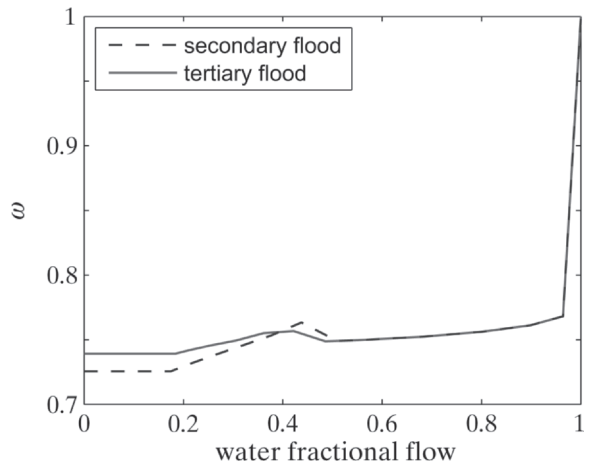

Fig. 14—Variation of the Todd and Longstaff (1972) parameter ω as a function of the injected water fractional flow.

Nomenclature

C = overall solvent volume fraction
C_l = injected solvent concentration
C_r = initial solvent concentration
f = water fractional flow
f_{inj} = injected water fractional flow
f_{opt} = optimum water fractional flow
$\hat{g}$ = solvent flux function
k_{rh} = hydrocarbon relative permeability
k_{rw} = water relative permeability
M = mobility contrast across the solvent front
M_{eff} = effective mobility ratio
S = water saturation
S_l = injected water saturation
S_{or} = residual oil saturation
S_r = initial water saturation
S_{wc} = connate water saturation
t = dimensionless time
U = unit composition triangle
u_l = injected composition state
u_m, u_t = intermediate composition states
u_r = initial composition state
W_R = WAG ratio
x = dimensionless space variable
ζ = x/t, characteristic speed
λ_h = mobility of the hydrocarbon phase
λ_w = mobility of the aqueous phase
λ_T = $\lambda_w+\lambda_h$, total mobility
μ_h = viscosity of the hydrocarbon phase
μ_o = oil viscosity
μ_s = solvent viscosity
μ_w = water viscosity
χ = solvent mass fraction in the hydrocarbon phase
ω = Todd and Longstaff parameter

References

Blunt, M. and Christie, M. 1993. How to predict viscous fingering in three component flow. *Transp. Porous Media* **12:** 207–236.

Blunt, M.J. and Christie, M. 1994. Theory of Viscous Fingering in Two-Phase, Three-Component Flow. *SPE Advanced Technology Series* **2** (2): 52–60.

Blunt, M.J. et al. 1994. Predictive Theory for Viscous Fingering in Compositional Displacement. *SPEREE* **9** (1): 73–80. SPE-24129-PA. DOI: 10.2118/24129-PA.

Buckley, S.E. and Leverett, M.C. 1942. Mechanism of Fluid Displacement in Sands. *Trans.,* AIME, **146:** 107–116.

Caudle, B.H. and Dyes, A.B. 1958. Improving Miscible Displacement by Gas–Water Injection. *JPT* **20** (11): 281–284; *Trans.,* AIME, **213.**

Chang, Y.-B., Lim, M.T., Pope, G.A., and Sepehrnoori, K. 1994. CO_2 Flow Patterns Under Multiphase Flow: Heterogeneous Field-Scale Conditions. *SPERE* **9** (3): 208–216. SPE-22654-PA. DOI: 10.2118/22654-PA.

Christie, M.A. 1989. High-Resolution Simulation of Unstable Flows in Porous Media. *SPERE* **4** (3): 297–303; *Trans.,* AIME, **287.** SPE-16005-PA. DOI: 10.2118/16005-PA.

Christie, M.A. and Bond, D.J. 1987. Detailed Simulation of Unstable Processes in Miscible Flooding. *SPERE* **2** (4): 514–522; *Trans.,* AIME, **283.** SPE-14896-PA. DOI: 10.2118/14896-PA.

Christie, M.A., Muggeridge, A.H., and Barley, J.J. 1993. 3D Simulation of Viscous Fingering and WAG Schemes. *SPERE* **8** (1): 19–26; *Trans.,* AIME, **295.** SPE-21238-PA. DOI: 10.2118/21238-PA.

Helfferich, F.G. 1981. Theory of Multicomponent, Multiphase Displacement in Porous Media. *SPEJ* **21** (1): 51–62. SPE-8372-PA. DOI: 10.2118/8372-PA.

Isaacson, E.L. 1980. Global solution of a Riemann problem for a non-strictly hyperbolic system of conservation laws arising in enhanced oil recovery. Technical Report. New York: The Rockefeller University.

Juanes, R. and Blunt, M.J. 2006. Analytical solutions to multiphase first-contact miscible models with viscous fingering. *Transp. Porous Media* **64** (3): 339–373. DOI: 10.1007/s11242-005-5049-z.

Juanes, R. and Lie, K.-A. 2005. A Front-Tracking Method for Efficient Simulation of Miscible Gas Injection Processes. Paper SPE 93298 presented at the SPE Reservoir Simulation Symposium, The Woodlands, Texas, 31 January–2 February. DOI: 10.2118/93298-MS.

Juanes, R. and Lie, K.-A. 2007. Numerical modeling of multiphase first-contact miscible flows. Part 1. Analytical Riemann solver. *Transp. Porous Media* **67** (3): 375–393. DOI: 10.1007/s11242-006-9031-1.

Juanes, R. and Lie, K.-A. In press. Numerical modeling of multiphase first-contact miscible flows. Part 2. Fronttracking/ streamline simulation. *Transp. Porous Media*. DOI: 10.1007/s11242-007-9139-y.

Koval, E.J. 1963. A Method for Predicting the Performance of Unstable Miscible Displacement in Heterogeneous Media. *SPEJ* **3** (3): 145–150; *Trans.,* AIME, **228.**

Lake, L.W. 1989. *Enhanced Oil Recovery*. Englewood Cliffs, New Jersey: Prentice-Hall.

Pope, G.A. 1980. The Application of Fractional Flow Theory to Enhanced Oil Recovery. *SPEJ* **20** (3): 191–205. SPE-7660-PA. DOI: 10.2118/7660-PA.

Smoller, J. 1994. *Shock Waves and Reaction-Diffusion Equations*. Second edition. Vol. 258 of *A Series of Comprehensive Studies in Mathematics*. New York: Springer-Verlag.

Stalkup, F.I. Jr. 1983. *Miscible Displacement*. SPE Monograph Series, vol. 8. Dallas: Society of Petroleum Engineers.

Tchelepi, H.A. and Orr, F.M. 1994. Interaction of Viscous Fingering, Permeability Heterogeneity, and Gravity Segregation in Three Dimensions. *SPERE* 9 (4): 266–271; *Trans.,* AIME, **297.** SPE-25235-PA. DOI: 10.2118/25235-PA.

Todd, M.R. and Longstaff, W.J. 1972. The Development, Testing, and Application of a Numerical Simulator for Predicting Miscible Flood Performance. *JPT* **24** (7): 874–882; *Trans.,* AIME, **253.**

Walsh, M.P. and Lake, L.W. 1989. Applying fractional flow theory to solvent flooding and chase fluids. *J. Pet. Sci. Eng.* **2:** 281–303.

Ruben Juanes is assistant professor of Civil and Environmental Engineering at the Massachusetts Institute of Technology. Before joining the MIT faculty in 2006, he was acting assistant professor in petroleum engineering at Stanford University, and assistant professor in petroleum and geosystems engineering at the University of Texas at Austin. His interest is in the theory and simulation of multiphase flow through porous media, with application to enhanced oil recovery by gas injection, geological CO_2 sequestration, and methane hydrates in ocean sediments. He holds MS and PhD degrees in civil and environmental engineering from the U. of California at Berkeley. **Martin J. Blunt** is Professor of Petroleum Engineering and head of the Department of Earth Science and Engineering at Imperial College, London. e-mail: m.blunt@imperial.ac.uk. He previously was an associate professor at Stanford University and worked at the BP Research Centre. He holds MA and PhD degrees in physics from Cambridge University. Blunt, winner of the 1996 Cedric K. Ferguson Medal, served as Associate Executive Editor of *SPEJ* from 1996–98 and was on the Editorial Board from 1996-2005. He is a member of the London Board of the SPE. Blunt was a 2001 Distinguished Lecturer.